Biointerface Research in Applied Chemistry
Platinum Open Access Journal (ISSN: 2069-5837)

Article
Volume 11, Issue 5, 2021, 12495 - 12505
https://doi.org/10.33263/BRIAC115.1249512505

Synthesis and Characterization of Lateral Fluoro-substituents Liquid Crystals

Beya Haouas [1], Tayssir Missaoui [2], Mohamed Ali Ben Aissa [1,*], Fathi Jomni [3], Youssef Arfaoui [4], Taoufik Soltani [5,*]

1 Université Tunis El-Manar Laboratoire de Chimie Analytique et Electrochimie, Faculté des Sciences de Tunis, Campus Universitaire 2092 Tunis, Tunisia
2 Université de Monastir, Laboratoire des interfaces et des matériaux avancés, Faculté des Sciences de Monastir, bd de l'environnement, 5019 Monastir, Tunisia
3 Université de Tunis El Manar, Laboratoire Matériaux Organisation et Propriétés (LR99ES17), 2092, Tunis, Tunisia
4 Laboratoire de Caractérisations, Applications et Modélisation de Matériaux(LR18ES08), Faculté des Sciences de Tunis, Université Tunis El-Manar, Campus Universitaire 2092 Tunis, Tunisia
5 Université de Tunis El Manar, Faculté des Sciences de Tunis, LR99ES16 Laboratoire Physique dela Matière Molle et de la Modélisation Électromagnétique, 2092 Tunis, Tunisia
* Correspondence: taoufik.soltani@ fst.utm.tn;

Scopus Author ID 18635127300
Received: 7.12.2020; Revised: 20.01.2021; Accepted: 24.01.2021; Published: 30.01.2021

Abstract: Lateral difluoro substituent liquid crystal based on a three-aromatic core has been synthesized. It has been designed to correlate the molecular structure and mesomorphism with reference to the difluoro substituent and -COO- linkage group. This compound was characterized by elementary analyses and spectroscopic techniques such as FTIR and ^{1}H-NMR. The synthesis compound's mesomorphic behavior was studied by polarizing optical microscope, differential scanning calorimetry, and dielectric measurements. The recent investigation reveals only SmB phase.

Keywords: difluoro liquid crystal; phase transitions; calorimetry; electrical; dielectrical properties.

1. Introduction

Liquid Crystals (LCs) have drawn significant attention. They are now one of the hot topics in LC research due to their fascinating and functional properties. The essential properties used to characterize a liquid-crystal are optical anisotropy, dielectric anisotropy, viscoelastic properties, phase stability, and research. The molecular structure influences these. Recent research has reported the synthesis of a wide range of mesogenic, in particular, fluorinated thermotropic liquid crystals [1-7]. Due to the combination of polar, steric effects and the great strength of the C-F bond, these materials have played an essential role in satisfying the exacting demands of the various types of liquid crystal displays. The influence of the lateral fluoro substituent on the mesophase behaviors of the ferroelectric and antiferroelectric LCs has been studied by several groups [8-10]. It has been found that the lateral fluoro substituent leads to the reduction of transition temperature and in the ferroelectric stability (SmC*). In contrast, more stability of the antiferroelectric SmCα has been observed compared to the non-fluoride series [11-12]. In general, for the non-chiral calamiticmesogens, the influence of lateral fluoro substituent on melting point, nematic and smectic stability, and anisotropic dielectric has been discussed with the result of enhancing some properties [13-19].

It is already known that the lateral mono and di-fluoro-substituent terphenyls have been used as host materials to give SmC* systems for ferroelectric display devices [20-24]. It has been found that the lateral fluoro-substituent in terphenyl systems enhances the stability of the tilted smectic phases and reduces the melting point. The difluorophenyl, which confer a high lateral dipole, shows an enhancement in negative dielectric anisotropy. To produce excellent host ferroelectric LC with lower viscosity, Hird has synthesized the terphenyl system with 2.3-difluoro substituent [25-26]. Then, the different positions of substitution must be distinguished.

In this work, we report the synthesis and mesomorphic properties of the lateral difluoro substituted terphenyl LC in an attempt to obtain a nematic phase with negative anisotropic dielectric and low viscosity. However, the differential scanning calorimetry and polarizing optical microscopic investigation reveal the following phase sequence: Cr-SmB-I.

2. Materials and Methods

2.1. Syntheticprocedures.

In the present work, the organic synthesis of the difluoro compound is illustrated in Figure 1. The 1,4-phenylene bis (2,3-difluoro-4-octyloxybenzoate) was synthesized by esterification of the 3,2-fluoro-4-octyloxybenzoic acid (2) with the hydroquinone (3) as described in [9]. The residue was purified by using column chromatography on silica gel eluting with toluene. The compound was recrystallized from absolute ethanol. The 2,3-difluoro-4-hydroxybenzoic acid (1) and the hydroquinone (3) were supplied by Sigma Aldrich. The compound (2) was prepared by the well-known method described in the reported literature [27].

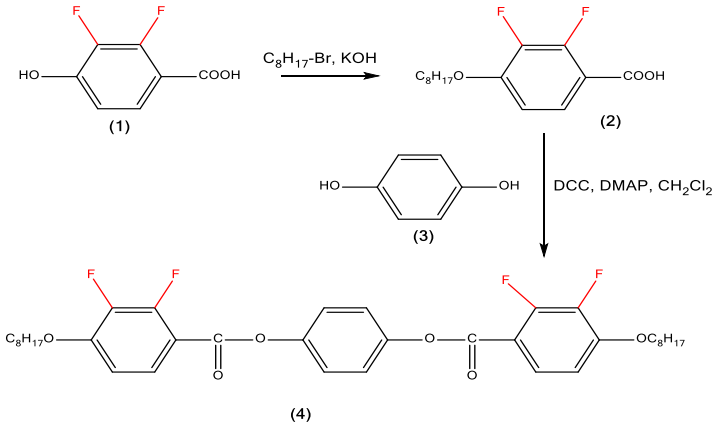

Figure 1. The synthetic route of the studied compound.

2.2. Characterization and computational details.

The synthesized product's chemical structure was characterized by Fourier transform infrared spectroscopy (FTIR) using Perkin-Elmer PARAGON 1000 PC and by nuclear magnetic resonance (NMR) spectroscopy on a Bruker AV 300 MHz Spectrometer.

All our theoretical calculations were performed using the GAUSSIAN09 program [28]. The geometry optimization was performed in DFT/B3LYP/6-31G(d). All geometrical parameters were allowed to vary independently apart from the planarity of the rings. A previous study shows that this method is well suited to the conformational analysis of conjugated molecules [29]. The harmonic vibration frequencies of the stationary points were calculated with the same basis to identify the local minima. Only the calculation of the frequencies makes it possible to control the nature of this stationary point.

To study the compound morphology, we loaded the obtained liquid crystal into ITO electro-optical cells (about 6 µm thick) by capillary action at the isotropic temperature. The temperature regulator was controlled by a programmable multimeter (Keithly Model 2000), a programmable DC power supply (HP E3632A), and an oven developed in our laboratory

The sample temperature was controlled using an oven with a precision better than ±0.1°C/min. Optical observations were made under a polarizing optical microscope (POM) (Olympus BX51) equipped with a digital CCD camera (Sony). Imaging software (Archimed) was used to process, analyze, and store the LC textures. The POM observations were correlated with differential scanning calorimetry (DSC) measurement using a Perkin-Elmer DSC7. To do this, DSC thermograms are obtained in the heating and cooling cycle. The sample is heated and cooled with a scan rate of 5°C/min and held at its isotropic phase for two minutes to attain thermal stability.

The dielectric measurements were performed using commercial cells (EHC,Japan) coated with indium tin oxide (ITO). The thickness of the cells is 6µm. The active area is 25 mm^2. The cells were filled with isotropic phase liquid crystals by capillary action. The dielectric measurements were performed using an impedance analyzer (SOLARTRON 1260) coupled with a dielectric interface 1296. Generally, the dielectric system response submitted to an external alternating electric field is governed, in the frequency domain, by the complex permittivity formalism (equation 1)

$$\varepsilon^*(\omega, T) = \varepsilon'(\omega, T) - i\,\varepsilon''(\omega, T) \quad (1)$$

Where ε'(ω, T) and ε″ (ω, T) are the real and imaginary parts of the complex permittivity, which represent the storage and the losses of the energy respectively during every electric field cycle. Several authors widely used this formalism of complex permittivity to identify the relaxation phenomena. The empirical Cole-Cole relaxation can express the nature of dielectric permittivity related to dipoles oscillating in an alternating field:

$$\varepsilon' = \varepsilon_\infty + \frac{(\varepsilon_S - \varepsilon_\infty)}{(1+(j\omega\tau)^{(1-\alpha)})} \quad (2)$$

Where ε_S and ε_∞ are the static and high frequency, respectively, $\omega(=2\pi f)$ is the angular frequency, τ is the relaxation time and α is constant $(0< \alpha<1)$

3. Results and Discussion

3.1. Molecular structure and supramolecular assembly.

The spectra were obtained using $CDCl_3$ as solvent and referenced to tetramethylsilane (TMS) as the internal standard (Figure 2).IR (KBr) ν (cm^{-1}) =2935, 2843 (C-H aliphatic), ν =1748 (C=O), ν =1000(C-F),) ν =1630, 1515, 1492, 1470 (C=C phenyl rings) (Figure 3).

The theoretical DFT/B3LYP/6-31G(d)calculation results, which are indicated in Figure 4, clearly illustrate that the two isomers S_1 and $S_3$are the most stable thermodynamically. The calculated Boltzmann distribution of the two S1 and S3 forms is 56% and 44%, respectively. The ^{19}F NMR spectrum decoupled from the proton shows that these forms are not equivalent either chemically or magnetically. The spectrum shows two systems of the AX type with the same ^2J coupling and equal to -19.7Hz [30].

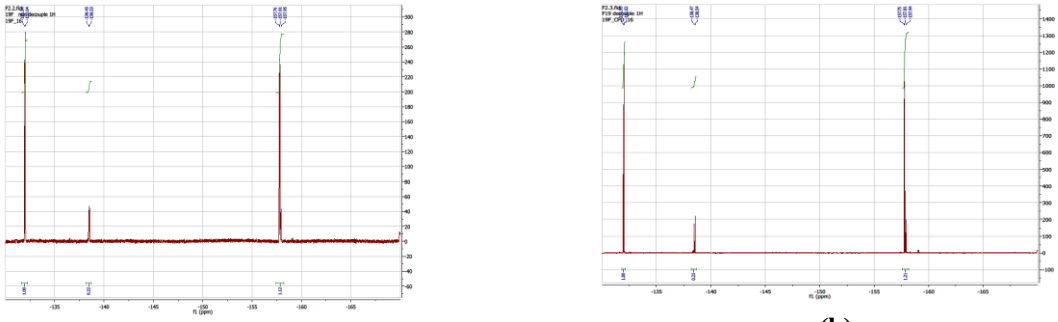

(**a**) (**b**)

Figure 2. NMR spectra of the studied molecule in $CDCl_3$:(**a**) S1: ^{19}F NMR not decoupled; (**b**) S2: NMR ^{19}F decoupled from ^{1}H spectrum.

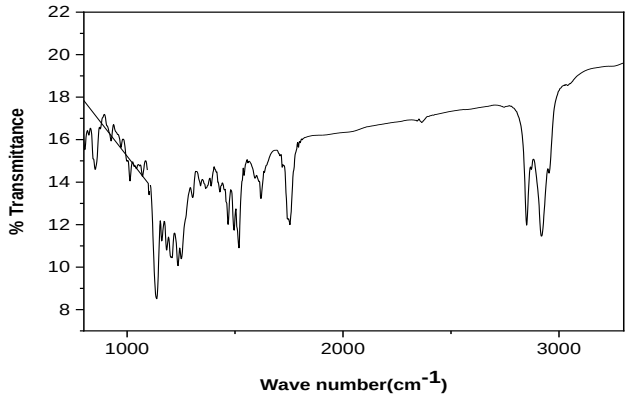

Figure 3. FTIR spectra of the studied compound.

The fluorine chemical shifts of the major isomer are -157.5 ppm for the A and -137,7 ppm for the X part, whereas, for the minor isomer, the chemical shifts are -157.6 ppm for the A and -138.4 ppm for the Xpart.experimentally, the yield of the major isomer S1 is 83%.

3.2.Phase diagram.

Differential scanning calorimetry (DSC) measurements were carried out on synthesized compounds under a nitrogen atmosphere to identify the phase transitions of LC. The temperature measurements varied between 25 and 175 °C with a heating and cooling rate of 5 °C/min. Figure 5 shows two endothermic peaks at 56.4°C and 101.5 °C, indicating that the present compound exhibits only one phase between crystal (Cr) and isotropic (I) phases.

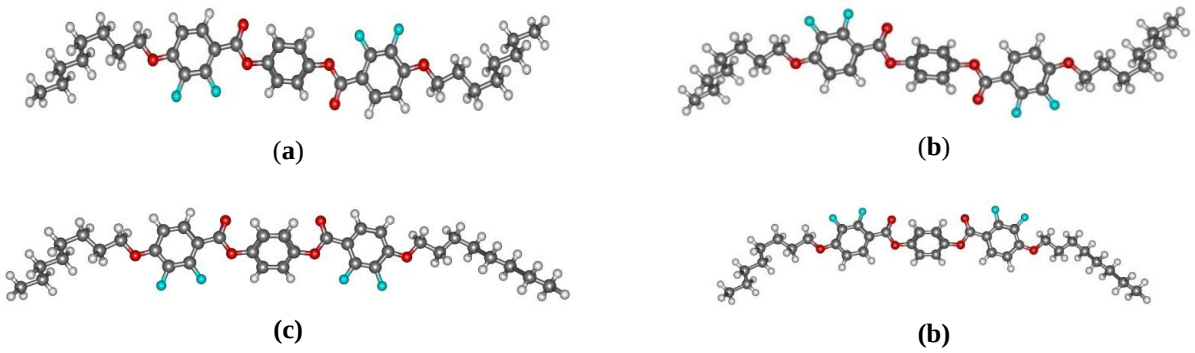

(**a**) (**b**)

(**c**) (**b**)

Figure 4. The four isomers structure and relatives' energies (kJ.mol^{-1}): (**a**):S_1(ΔE= 0 kJ.mol^{-1}); (**b**):S_2 (ΔE= 12.03kJ.mol^{-1}); (**c**):S_3(ΔE = 0.535 kJ.mol^{-1}); (d): S_4 (ΔE= 14.03 kJ.mol^{-1}).

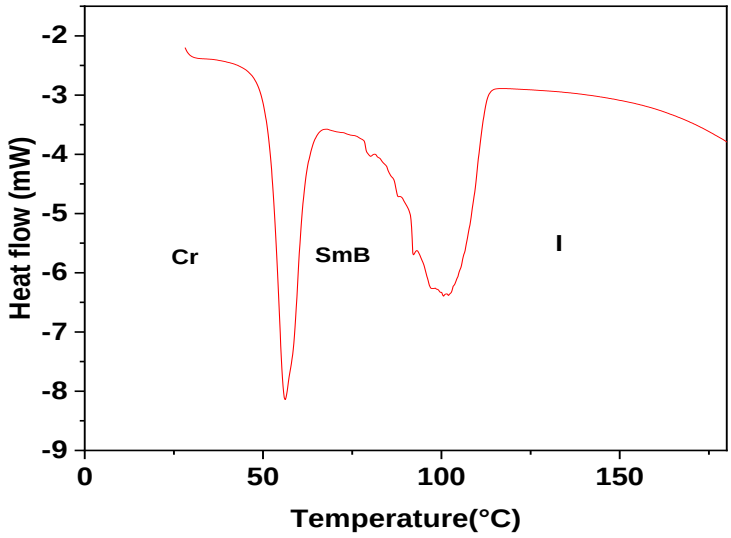

Figure 5. DSC diagram at a heating rate of 5°C min^{-1}.

Also, by using a polarizing optical microscope (POM), the phase transition temperatures and the texture of LC mesogens were observed. Figure 6(a) shows the lancets and pseudo isotropic regions formed just below the isotropic temperature, which is generally an indication of the smectic B. At 56.5°C, the isotropic regions may be due to the homeotropically oriented molecules. Figure 6(b) depicts the coexistence of both phases, SmB, with crystalline, indicating the first characteristic order of this transition. According to the DSC analysis and the POM observations, we can conclude that the synthesized compound exhibits the following phase sequence: Cr-SmB-I. The associated enthalpies obtained from DSC thermograms and thus associated entropy of the prepared compound are given in Table 1. Therefore, the two-phase transitions have a substantially larger latent heat and can be interpreted as the strongest first-order. In addition, the large peak at the I-SmB obtained by the DSC measurements (Fig.5) is due to the very slow transformation of the isotropic phase to the SmB. This behavior is consistent with the observed SmC-SmB-K phase sequence in CNT/LCs system by Klonkanda *et al*. [31]. They have demonstrated that both the SmC-SmB and SmB-K phase transitions are strongly first order, and the SmC was slowly transformed to the SmB. Moreover, a large peak at the transition SmB-I has been observed in the F8H6F8 system [32].

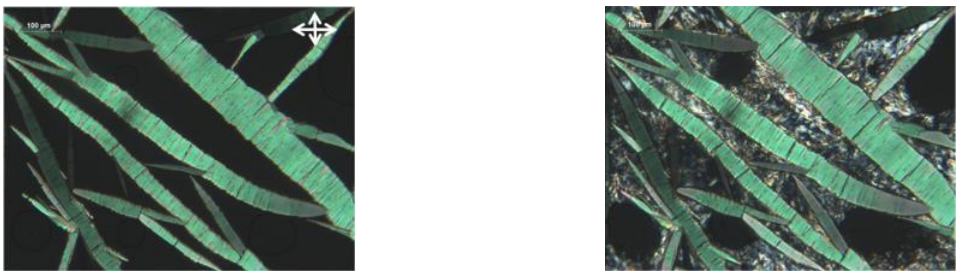

(**a**) (**b**)

Figure 6. Morphological textures: (a) SmB phase and (b) coexistence (SmB and crystalline phases).

Table1. Enthalpy and entropy change corresponding to various peaks observed in the DSC thermogram.

	Cr-SmB	**SmB-I**
T(°C)	56.4	101.5
$\Delta \boldsymbol{H}$5(k J.mol^{-1})	3.63	6.84
$\Delta \boldsymbol{S}$(J.K-1.mol^{-1})	11.02	18.26

3.3. Electrical and dielectric properties

The dielectric study was performed on a planar cell of 6μm thickness in the frequency range of 10 Hz-1MHz on cooling the sample from 100°C to 55°C. Figure 7 illustrates the frequency evolution of the imaginary part of the dielectric permittivity.

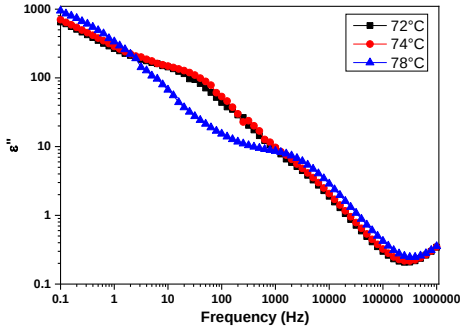

Figure 7. Frequency dependence of the imaginary part ε" of the dielectric permittivity at 72°C, 74°C, and 78°C.

At the low-frequency region, the dielectric behavior is dominated by the ionic contribution. Also, the low-frequency relaxation is attributable to the space-charge polarization resulting from the migration of mobile ions. It is important to signal that increases with increasing temperature, which can be explained by promoting the ion transport at higher temperatures or increasing the number of charge carriers contributing to electric conduction in the cells. These increases suggested an increase in the conductivity of the sample according to the well-known proportionality $\sigma = \varepsilon_0 \omega \varepsilon''$[34-35].A plot of log (σ) with respect to the inverse temperature exhibited an Arrhenius-type behavior (Equation 3), as shown in Figure 8.

$$\sigma = \sigma_0 e^{\left(\frac{-E_a}{K_B T}\right)} \quad (3)$$

Where E_a denotes the thermal activation energy of electrical conduction that depends on the conductor's nature, σ_0 denotes the conductivity value when the reciprocal of temperature tends to zero, and k_B is the Boltzmann constant. The activation energy obtained from the slope was E_a = 6.7 eV. This value is of the same order of magnitude for hydrogen-bonded liquid crystal[16]and higher than 0.6 eV measured in the antiferroelectric liquid crystal [35].

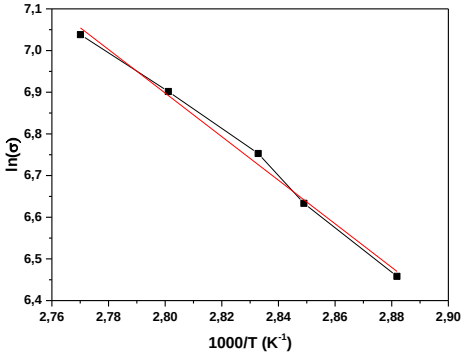

Figure 8. The electric conductivity of the sample in the 70°-86°C temperature range.

Impedance Spectroscopy is a powerful method to investigate mobile charges' behavior in the liquid crystal's bulkor interfacial regions [36-42]. Therefore, both real (*Zr*) and imaginary (*Zi*) parts of the complex electrical impedance (*Z**) were simultaneously measured as a function of the frequency (*f*) and as the temperature. The Nyquist plots (*Zi* versus *Zr*) for the studied samples demonstrated semi-circular arcs, as seen in Figure 9.

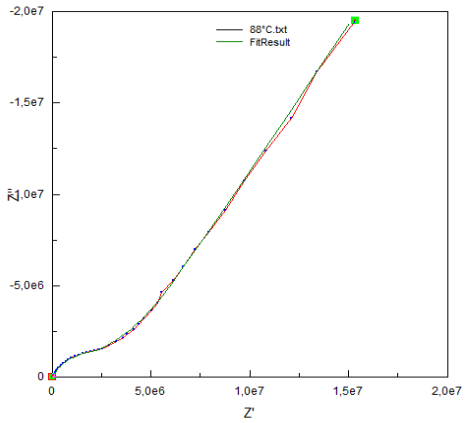

Figure 9. Nyquist representation of the complex impedance of the synthesized compound.

To evaluate the ion behaviors near the bulk and surface region, we used an equivalent circuit that reproduces the experimental Nyquist data, as illustrated in Figure 10. This latter comprises the resistance, capacitance, and Warburg impedance, as shown in Figure 9. The generalized finite-length Warburg impedance (Z_W) can be expressed as[43-45]:

$$Z_W = \frac{W_{Sr}}{\sqrt{iw}}(1-i)tnh\left(W_{Sc}\sqrt{iw}\right) \quad (4)$$

Where the parameters W_{Sr} and W_{Sc} can be expressed as:

$$W_{Sr} = \frac{RTN_A}{F^2An_S\sqrt{2D}} \quad (5)$$

$$W_{Sc} = \frac{\delta_N}{\sqrt{D}} \quad (6)$$

where ω is the angular frequency, R is the gas constant, T is the temperature, N_A is the Avogadro's number, F is the Faraday constant, A is the surface area, n_s is the surface concentration of the ions, D is the diffusion coefficient of the mobile ions, and δ_N is the thickness of the Nernst diffusion layer.

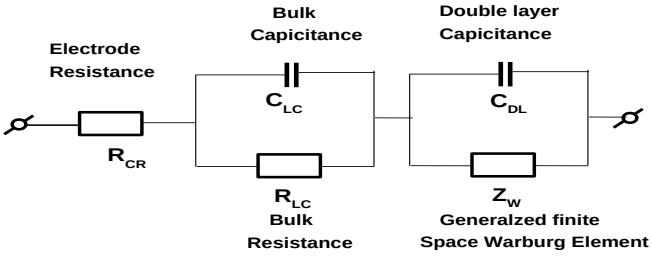

Figure 10. Equivalent electric circuit for the liquid crystal 8CB and 8CB + NPs.

The EEC's electrical parameters are obtained by fitting the experimental data and are summarized in Table 2.

Table 2. Impedance spectroscopy parameters as the elements of the EEC model were obtained by using the measured impedance spectra.

T (°C)	R_{cr} (Ω)	C_{LC} (pF)	R_{LC} (Ω)	C_{DL} (nF)	W_{SC}(Ω·s$^{-1/2}$)	W_{SR}(MΩ·s$^{-1/2}$)
74	891	59.5	236460	31.35	0,941	73.76
78	1011	61.6	140670	34.3	0,686	37.7

From this table, we can conclude that the electrode resistance R_S, which represents the resistance of connectors and electrodes, is slightly affected by the temperature. In addition, the capacitance of the bulk C_{LC} remains constant, while the bulk resistance R_{LC} decreases with

increasing temperature. This increase in $R_{LC}$is due to the increase in conductivity. This observation is in good agreement with the dielectric measurement. Also, the double-layer capacitance C_{DL}, which is higher than the bulk capacitance C_{LC} increases the temperature. It should be mentioned that this temperature-sensitive component in the EEC is quite useful for designing liquid crystal temperature.

Figure11 presents the temperature dependence of the real permittivity (ε') of the studied compound at 2 kHz, which shows significant changes at 100°C and 58°C indicating the I - SmB and SmB - Crystal phase transitions, respectively. This result is in good agreement with the POM and the DSC measurements. The increase of the real permittivity at the I-SmBphase transition can be attributed to the dielectric and the elastic anisotropy of SmB.

In fact, the influence of the lateral fluoro substituent on the nematic phase's stability and the improvement of the physical properties have been investigated by different authors. For example, the nematic phase with a higher value of negative dielectric anisotropy has been observed in the compound with three benzenes and four lateral fluoro substituents required for some display applications [20]. However, in this case, the stability of the nematic phase is less than desired. To increase the nematic stability and maintain the negative dielectric anisotropy, in the present work, we modified the chemical structure of these compounds studied in reference [46]by introducing the ester function (CO_2) as a linking group.

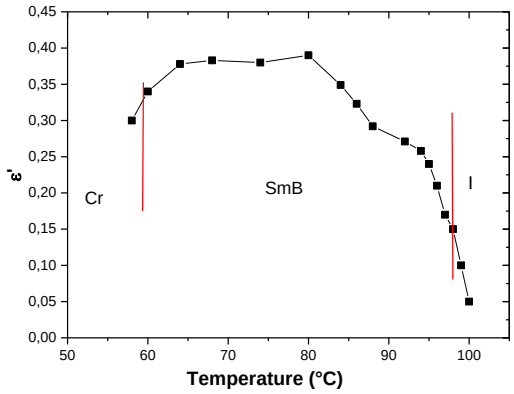

Figure 11. Temperature dependence of the real part(ε') of the dielectric permittivity at 2kHz.

It is important to note that the ester extends the molecular length and enhances the polarizability anisotropy, which increases the liquid crystal thermal stability. Also, in the present compound, the molecular structure is quite symmetrical, with identical terminal chains. The nematic phase is expected. However, this structure excludes the nematic phase and allowing the SmB phase to be generated.

The appearance of the ordered SmB phase may be due to the combination of the polarity of the lateral difluoro substituents, the ester as a linking group, and the ether oxygen in the terminal chain, such as this phase has been observed in the unsubstituent compound with ether function [47].

4. Conclusions

In summary, we have synthesized a lateral fluoro substituents liquid crystal. The mesogenic behavior of the synthesized compound was measured by POM and DSC studies. The phase-transition sequence of this compound has been found to be: Cr-SmB-I. Our experiments show that both Gr-SmB and SmB-I phase transitions are strongly first order. The phase transition temperature values obtained from the dielectric measurements agree with those

obtained by POM and DSC experiments. The DFT calculation shows two possible thermodynamically stable isomers. The obtained theoretical Boltzmann distribution was in good agreement with the experimental one. The use of four fluoro substituents in the aromatic core, in addition to those already present in ester function as a linked group, results in the appearance of smectic B. This study will help in exploring additional possibilities to design and synthesized several supramolecular with stable LC phases.

Funding

This research received no external funding.

Acknowledgments

This research has no acknowledgment.

Conflicts of Interest

The authors declare no conflict of interest.

References

1. Stevenson, W.D.; Zou, H.-x.; Zeng, X.-b.; Welch, C.; Ungar, G.; Mehl, G.H. Dynamic calorimetry and XRD studies of the nematic and twist-bend nematic phase transitions in a series of dimers with increasing spacer length. *Physical Chemistry Chemical Physics* **2018**, *20*, 25268-25274, https://doi.org/10.1039/C8CP05744C.
2. Kaur, S.; Liu, H.; Addis, J.; Greco, C.; Ferrarini, A.; Görtz, V.; Goodby, J.W.; Gleeson, H.F. The influence of structure on the elastic, optical and dielectric properties of nematic phases formed from bent-core molecules. *Journal of Materials Chemistry C* **2013**, *1*, 6667-6676, https://doi.org/10.1039/C3TC31545B.
3. Lin, Y.-H.; Ezhumalai, Y.; Yang, Y.-L.; Liao, C.-T.; Hsu, H.-F.; Wu, C. Influence of Mesogenic Properties of Cruciform-Shaped Liquid Crystals by Incorporating Side-Arms with a Laterally-Substituted-Fluorine. *Crystals* **2013**, *3*, 339-349, https://doi.org/10.3390/cryst3020339.
4. Gauza, S.; Li, J.; Wu, S.T.; Spadło, A.; Da˛browski, R.; Tzeng, Y.N.; Cheng, K.L. High birefringence and high resistivity isothiocyanate-based nematic liquid crystal mixtures. *Liquid Crystals* **2005**, *32*, 1077-1085, https://doi.org/10.1080/02678290500303007.
5. Kumar, J.; Prasad, V. Ferroelectric Nematic and Ferrielectric Smectic Mesophases in an Achiral Bent-Core Azo Compound. *The Journal of Physical Chemistry B* **2018**, *122*, 2998-3007, https://doi.org/10.1021/acs.jpcb.7b11733.
6. Pytlarczyk, M.; Dmochowska, E.; Czerwiński, M.; Herman, J. Effect of lateral substitution by chlorine and fluorine atoms of 4-alkyl-p-terphenyls on mesomorphic behaviour. *Journal of Molecular Liquids* **2019**, *292*, https://doi.org/10.1016/j.molliq.2019.111379.
7. Mabrouki, A.; Fouzai, M.; Soldera, A.; Kriaa, A.; Hedhli, A. Synthesis, liquid crystalline behaviour and structure–propertyrelationships of 1, 3-bis (5-substituted-1, 3, 4-oxadiazol-2-yl) benzenes. *Beilstein journal of organic chemistry* **2020**, *16*, 149-158,https://doi.org/10.3762/bjoc.16.17.
8. Gupta, D.; Kula, P.; Bhattacharjee, A. Mesomorphic, electro-optic and dielectric behaviour of a semi-fluorinated chiral liquid crystalline material forming polar smectic phases. *Journal of Molecular Structure* **2020**, *1219*,https://doi.org/10.1016/j.molstruc.2020.128557.
9. Dey, K.C.; Mandal, P.K.; Kula, P. Effect of fluorinated achiral chain length on structural, dielectric and electro-optic properties of two terphenyl based antiferroelectric liquid crystals. *Journal of Molecular Liquids* **2020**, *298*, https://doi.org/10.1016/j.molliq.2019.112056.
10. Herman, J.; Aptacy, A.; Dmochowska, E.; Perkowski, P.; Kula, P. The effect of partially fluorinated chain length on the mesomorphic properties of chiral 2',3'-difluoroterphenylates. *Liquid Crystals* **2020**, https://doi.org/10.1080/02678292.2020.1811410.
11. Zang, X.-Y.; Gao, L.; Zhang, R.; Dong, L.; Chen, X.-S.; Li, Y.-N.; Yao, D.-S.; Hu, J.-S.; Jia, Y.-G.; Li, F.-H.; Tian, M. Fluorinated chiral nematic liquid crystal dimers based on (S)-1-phenylethane-1,2-diol. *Liquid Crystals* **2020**, *47*, 689-701, https://doi.org/10.1080/02678292.2019.1673907.
12. Essid, S.; Manai, M.; Gharbi, A.; Marcerou, J.P.; Rouillon, J.C.; Nguyen, H.T. Synthesis and characterization of a novel liquid crystal series with tribenzoate cores and monofluoro-substitution on the phenyl ring near the chiral chain. *Liquid Crystals* **2004**, *31*, 1185-1193,https://doi.org/10.1080/02678290410001648651.

13. Cruz, C.D.; Rouillon, J.C.; Marcerou, J.P.; Isaert, N.; Nguyen, H.T. Synthesis and mesomorphic properties of a new chiral series with anticlinic and TGB phases. *Liquid Crystals* **2001**, *28*, 125-137, https://doi.org/10.1080/026782901462463.
14. Soltani, T.; Bitri, N.; Dhaouadi, H.; Gharbi, A.; Marcerou, J.P.; Nguyen, H.T. Synthesis, characterisation and behaviour under a field of a chiral smectic liquid crystal. *Liquid Crystals* **2009**, *36*, 1329-1336, https://doi.org/10.1080/02678290903220998.
15. Cruz, C.D.; Rouillon, J.C.; Marcerou, J.P.; Isaert, N.; Nguyen, H.T. Influence of the position and number of fluorine atoms and of the chiral moiety on a newly synthesized series with anticlinic properties. *Liquid Crystals* **2001**, *28*, 1185-1192, https://doi.org/10.1080/02678290110048778.
16. Fouzai, M.; Hamdi, R.; Ghrab, S.; Soltani, T.; Ionescu, A.; Othman, T. Properties of binary mixtures derived from hydrogen bonded liquid crystals. *Journal of Molecular Liquids* **2018**, *249*, 1279-1286, https://doi.org/10.1016/j.molliq.2017.11.128.
17. Kelly, S.M. The synthesis and transition temperatures of benzoate ester derivatives of 2-fluoro-4-hydroxy- and 3-fluoro-4-hydroxybenzonitriles. *Helvetica Chimica Acta* **1984**, *67*, 1572-1579, https://doi.org/10.1002/hlca.19840670623.
18. McDonnell, D.G.; Raynes, E.P.; Smith, R.A. Dipole moments and dielectric properties of fluorine substituted nematic liquid crystals. *Liquid Crystals* **1989**, *6*, 515-523, https://doi.org/10.1080/02678298908034171.
19. Dãbrowski, R.; Dziaduszek, J.; Drzewiński, W.; Czupryński, K.; Stolarz, Z. Synthesis and Mesomorphic Characteristic of Bicyclo-(2,2,2)Octane Derivatives with the -NCS Terminal Group. *Molecular Crystals and Liquid Crystals Incorporating Nonlinear Optics* **1990**, *191*, 171-176, https://doi.org/10.1080/00268949008038589.
20. Fouzai, M.; Guesmi, A.; Hamadi, N.B.; Soltani, T. Fluoro-substitution in hydrogen bonding liquid crystal benzoic acid: dielectric, electro-optic and optical proprieties and inducing polar nematic phase. *Liquid Crystals* **2020**, *47*, 777-784,https://doi.org/10.1080/02678292.2019.1679900.
21. Missaoui, T.; Ben Amor, I.; Soltani, T.; Ben Ouada, H.; Jeanneau, E.; Chevalier, Y. Dielectric and electro-optic properties of cybotactic nematic phase in hydrogen-bonded liquid crystals. *Journal of Molecular Liquids* **2020**, *304*,https://doi.org/10.1016/j.molliq.2020.112726.
22. Hird, M.; Toyne, K.J.; Gray, G.W. The synthesis and transition temperatures of some ferroelectric host materials based on 4- and 4′-(trans-4-alkylcyclohexylmethoxy)-2,3-difluorobiphenyls. *Liquid Crystals* **1994**, *16*, 625-641,https://doi.org/10.1080/02678299408036535.
23. Zhou, Y.; Patterson, R.; Palmer, B.A.; Edwards-Gau, G.R.; Kariuki, Benson M.; Kumar, N.S.S.; Bruce, D.W.; Dolbnya, I.P.; Collins, S.P.; Malandain, A.; Harris, K.D.M. Spatially resolved mapping of phase transitions in liquid-crystalline materials by X-ray birefringence imaging. *Chemical Science* **2019**, *10*, 3005-3011, https://doi.org/10.1039/c8sc05285a.
24. Dmochowska, E.; Bombalska, A.; Kula, P. Synthesis and mesomorphic properties of four ring, rod-like fluorene derivatives – the influence of the lateral substitution on mesomorphic properties of 2,7-bis(4-alkylphenyl)-fluorenes. *Liquid Crystals* **2020**, *47*, 17-27,https://doi.org/10.1080/02678292.2019.1622047.
25. Alaasar, M.; Schmidt, J.-C.; Darweesh, A.F.; Tschierske, C. Azobenzene-based supramolecular liquid crystals: The role of core fluorination. *Journal of Molecular Liquids* **2020**, *310*,https://doi.org/10.1016/j.molliq.2020.113252.
26. Jasiurkowska-Delaporte, M.; Rozwadowski, T.; Juszyńska-Gałązka, E. Kinetics of Non-Isothermal and Isothermal Crystallization in a Liquid Crystal with Highly Ordered Smectic Phase as Reflected by Differential Scanning Calorimetry, Polarized Optical Microscopy and Broadband Dielectric Spectroscopy. *Crystals* **2019**, *9*,https://doi.org/10.3390/cryst9040205.
27. Chu, J.; Wu, L.; Guo, Y.; Li, Y.; Li, B.; Yang, Y. A series of fluorinated liquid crystals with an alanine residue. *Liquid Crystals* **2020**, *47*, 465-470, https://doi.org/10.1080/02678292.2019.1690061.
28. Gupta, D.; Kula, P.; Bhattacharjee, A. Mesomorphic, electro-optic and dielectric behaviour of a semi-fluorinated chiral liquid crystalline material forming polar smectic phases. *Journal of Molecular Structure* **2020**, *1219*, https://doi.org/10.1016/j.molstruc.2020.128557.
29. Lalik, S.; Deptuch, A.; Fryń, P.; Jaworska–Gołąb, T.; Dardas, D.; Pociecha, D.; Urbańska, M.; Tykarska, M.; Marzec, M. Systematic study of the chiral smectic phases of a fluorinated compound. *Liquid Crystals* **2019**, *46*, 2256-2268, https://doi.org/10.1080/02678292.2019.1622044.
30. Hird, M.; Toyne, K.J.; Slaney, A.J.; Goodby, J.W. Synthesis and transition temperatures of host materials for ferroelectric mixtures. *Journal of Materials Chemistry* **1995**, *5*, 423-430, https://doi.org/10.1039/jm9950500423.
31. Hird, M. Fluorinated liquid crystals – properties and applications. *Chemical Society Reviews* **2007**, *36*, 2070-2095, https://doi.org/10.1039/b610738a**.**
32. Nguyen, H.T.; Rouillon, J.C.; Cluzeau, P.; Sigaud, G.; Destrade, C.; Isaert, N. New chiral thiobenzoate series with antiferroelectric mesophases. *Liquid Crystals* **1994**, *17*, 571-583, https://doi.org/10.1080/02678299408036741.
33. Frisch, M.J.; Trucks, G.W.; Schlegel, H.B.; Scuseria, G.E.; Robb, M.A.; Cheeseman, J.R.; Scalmani, G.; Barone, V.; Mennucci, B.; Petersson, G.A.; Nakatsuji, H.; Caricato, M.; Li, X.; Hratchian, H.P.; Izmaylov,

A.F.; Bloino, J.; Zheng, G.; Sonnenberg, J.L.; Hada, M.; Ehara, M.; Toyota, K.; Fukuda, R.; Hasegawa, J.; Ishida, M.; Nakajima, T.; Honda, Y.; Kitao, O.; Nakai, H.; Vreven, T.; Montgomery, J.A.; Peralta, J.E.; Ogliaro, F.; Bearpark, M.; Heyd, J.J.; Brothers, E.; Kudin, K.N.; Staroverov, V.N.; Kobayashi, R.; Normand, J.; Raghavachari, K.; Rendell, A.; Burant, J.C.; Iyengar, S.S.; Tomasi, J.; Cossi, M.; Rega, N.; Millam, J.M.; Klene, M.; Knox, J.E.; Cross, J.B.; Bakken, V.; Adamo, C.; Jaramillo, J.; Gomperts, R.; Stratmann, R.E.; Yazyev, O.; Austin, A.J.; Cammi, R.; Pomelli, C.; Ochterski, J.W.; Martin, R.L; Morokuma, K.; Zakrzewski, V.G.; Voth, G.A.; Salvador, P.; Dannenberg, J.J.; Dapprich, S.; Daniels, A.D.; Farkas, Ö.; Foresman, J.B.; Ortiz, J.V.; Cioslowski, J.; Fox, D.J. Gaussian 09. Gaussian, Inc., Wallingford CT. **2009**.

34. Haloui, A.; Arfaoui, Y. A DFT study of the conformational behavior of para-substituted acetophenones in vacuum and in various solvents. *Journal of Molecular Structure: Theochem* **2010**, *950*, 13-19, https://doi.org/10.1016/j.theochem.2010.03.012.
35. Castillo, N.; Matta, C.F.; Boyd, R.J. Fluorine−Fluorine Spin−Spin Coupling Constants in Aromatic Compounds: Correlations with the Delocalization Index and with the Internuclear Separation. *Journal of Chemical Information and Modeling* **2005**, *45*, 354-359, https://doi.org/10.1021/ci0497051.
36. Kalakonda, P.; Basu, R.; Nemitz, I.R.; Rosenblatt, C.; Iannacchione, G.S. Studies of nanocomposites of carbon nanotubes and a negative dielectric anisotropy liquid crystal. *The Journal of Chemical Physics* **2014**, *140*, https://doi.org/10.1063/1.4867791.
37. Chachaj-Brekiesz, A.; Górska, N.; Osiecka, N.; Mikuli, E.; Dynarowicz-Łątka, P. Synthesis and thermal behavior of triblock semifluorinated n-alkanes. *Journal of Thermal Analysis and Calorimetry* **2016**, *124*, 251-260, https://doi.org/10.1007/s10973-015-5149-0.
38. Özgan, Ş.; Eskalen, H. Electrical properties of the octyl cyanobiphenyl nematic liquid crystal dispersed with graphene oxide. *Journal of Materials Science: Materials in Electronics* **2020**, *31*, 19787-19796, https://doi.org/10.1007/s10854-020-04503-3.
39. Nepal, S.; Das, B.; Das, M.K.; Strójwąs, K.; Urbańska, M. Dielectric spectroscopy and electrical conductivity measurements on high-tilted antiferroelectric materials. *Phase Transitions* **2020**, *93*, 909-923, https://doi.org/10.1080/01411594.2020.1813288.
40. Marzal, V.; Caño-García, M.; Torres, J.C.; Quintana, X.; Pérez, I.; Garcia-Camara, B. Electrical Behavior of Liquid Crystal Devices with Dielectric Nanoparticles. *Journal of Nanomaterials* **2020**, *2020*, https://doi.org/10.1155/2020/4515432.
41. Mrukiewicz, M.; Perkowski, P.; Urbańska, M.; Węgłowska, D.; Piecek, W. Electrical conductivity of ion-doped fluoro substituted liquid crystal compounds for application in the dynamic light scattering effect. *Journal of Molecular Liquids* **2020**, *317*, https://doi.org/10.1016/j.molliq.2020.113810.
42. Urbanski, M.; Lagerwall, J.P.F. Nanoparticles dispersed in liquid crystals: impact on conductivity, low-frequency relaxation and electro-optical performance. *Journal of Materials Chemistry C* **2016**, *4*, 3485-3491, https://doi.org/10.1039/C6TC00659K.
43. Zafra, J.C.T.; Garcilópez, I.A.P.; Del Pozo, V.U.; Pena, J.M.S.; Lucas, C.M. Electrical modeling of tristate antiferroelectric liquid crystal devices. *Optical Engineering* **2011**, *50*, https://doi.org/10.1117/1.3564817.
44. Belyaev, B.A.; Drokin, N.A. Impedance spectroscopy investigation of electrophysical characteristics of the electrode-liquid crystal interface. *Physics of the Solid State* **2015**, *57*, 181-187, https://doi.org/10.1134/S1063783415010060.
45. Dalir, N.; Javadian, S.; Kakemam, J.; Yousefi, A. Evolution of electro-chemical and electro-optical properties of nematic liquid crystal doped with graphene oxide. *Journal of Molecular Liquids* **2018**, *265*, 398-407, https://doi.org/10.1016/j.molliq.2018.05.138.
46. Pauluth, D.; Tarumi, K. Advanced liquid crystals for television. *Journal of Materials Chemistry* **2004**, *14*, 1219-1227, https://doi.org/10.1039/b400135b.
47. Sackmann, H. Fliissigo Kristalle in Tabellen. *Zeitschriftfür Chemie* **1974**, *14*, 295-295.